AIMS Energy, 13(4): 879–900.
DOI: 10.3934/energy.2025032
Received: 25 April 2025
Revised: 25 June 2025
Accepted: 15 July 2025
Published: 23 July 2025

http://www.aimspress.com/journal/energy

Research article

Research on the modeling and simulation of the rural Photovoltaic-Biogas-Storage Direct-Current and Flexible Architecture System

Yingjie Wang[1,2,3], Shijie Li[1,2], Yi Zhao[1,2,*], Shuailei Kang[1,2] and Guanghui Chu[1,2]

[1] School of Intelligent Construction and Civil Engineering, Zhongyuan University of Technology, No. 41 Zhongyuan Road (M), Zhengzhou, China
[2] Henan Engineering Research Center of Mechanics and Engineering Structures, Zhongyuan University of Technology, No. 41 Zhongyuan Road (M), Zhengzhou, China
[3] Henan Province Engineering Research Center of Efficient use of new energy of low carbon technologies, Henan Mechanical and Electrical Vocational College, Zhengzhou South University City, Zhengzhou, China

* **Correspondence:** Email: 6357@zut.edu.cn; Tel: +15890101639.

Abstract: Under the dual carbon goals, the rapid advancement of rural energy transition and development highlights the imperative need for the integration of rural energy resources. Integrating rural energy resources is critical to address the mismatch between photovoltaic generation capacity and load demand in energy transition. In this study, we innovatively proposed a Photovoltaic-Biogas-Storage Direct-Current and Flexible Architecture System (PBS-DC-FAS), which combined photovoltaic (PV), biogas power generation, energy storage, heating, ventilation, and air conditioning (HAVC), and direct current (DC)-based building energy utilization. Modular modeling methods were applied to establish subsystem models and grid interaction strategies. These models and strategies were validated through a case study of Xiaohe Village's residential renovation project, employing MATLAB simulations. Meticulous attention was given to calibrating foundational data, considering meteorological conditions, and determining evaluation metrics during the validation process. Results demonstrated that the system significantly outperformed conventional systems in terms of energy flexibility, operational economy (electricity costs), carbon reduction, and stability (voltage fluctuation). The integration of multi-energy coupling and DC flexible architecture resolved rural energy supply-demand conflicts and enhanced grid resilience. We provided a replicable framework for rural decarbonization through localized energy synergy and DC-driven flexibility.

Keywords: PV-Biogas-Storage DC Flexible System; rural revitalization; rural areas with new energy; energy transformation

1. Introduction

In the pursuit of "dual carbon" objectives, namely, achieving carbon peaking and carbon neutrality, the landscape of energy technology has witnessed a paradigm shift, with the deployment of new energy technologies proliferating across sectors. This transformative era is also characterized by the relentless refinement and groundbreaking innovations in power systems, aimed at fostering a sustainable energy future. National policy frameworks underscore a significant uptick in the integration of renewable energy sources such as wind, solar, biomass, and geothermal energies into rural energy portfolios. As a result, the resilience and reliability of rural power grids have been fortified, paving the way for the exponential growth of distributed renewable energy infrastructure. This surge in clean energy adoption has, in turn, catalyzed the widespread proliferation of green and low-carbon business models and entrepreneurial ventures [1]. The green and low-carbon transformation of rural energy systems focuses on the multi-energy complementary utilization of renewable energy to construct multi-agent collaborative operation mechanisms, collaborative planning models for multi-energy systems, and design optimization models for zero-carbon integrated energy systems, while exploring the analysis of energy system morphological characteristics and optimal scheduling of multi-energy coupling [2–5]. The new energy sector has emerged as a linchpin in rural economic development, offering a vital complement to traditional revenue streams and serving as a catalyst for augmenting farmers' livelihoods. This dynamic synergy is propelling the rapid construction of a green, multifaceted, and sustainable rural energy ecosystem, heralding a new era of energy autonomy and environmental stewardship in rural communities.

The urgent demand for multi-energy synergy technology in the low-carbon transformation of rural building energy systems. The harmonious integration and optimization of photovoltaics (PV), biogas, and energy storage systems have surfaced as a pivotal pathway for augmenting energy utilization efficiency. The "Photovoltaics-Biogas-Storage Direct Current Flexible" (PBS-DCF) building framework is embodied as an integrated solution of multi-energy coupling, the term "PV" encapsulates distributed photovoltaic installations, "Biogas" embodies biogas-based initiatives, "Storage" denotes energy storage mechanisms, "Direct Current" (DC) underscores the system's adoption of direct current power distribution, and "Flexible" epitomizes the attainment of adaptable electricity consumption patterns [6]. The PBS-DCF building system endeavors to curtail users' electricity expenditures and mitigate grid load fluctuations by orchestrating the synergy among photovoltaic, biogas, energy storage, electric vehicle charging, and heating, ventilation, and air conditioning (HVAC) [7]. In pursuit of low-carbon building operations, it is imperative to amalgamate photovoltaic power output prognostication with flexible load management strategies across diverse temporal dimensions [8].

At present, research on the coupling effects of multiple energy sources is incomplete. Scholarly works such as these furnish a foundational bedrock for residential energy integration through dynamic simulations and empirical validations anchored in Geographic Information Systems (GIS) [9]. Dong et al. [10] introduced a dynamic optimal power flow algorithm tailored for low-voltage distribution networks that seamlessly incorporates photovoltaics and energy storage solutions. Tang A et al. [11] delineated a synergistic amalgamation of biogas power generation and a pioneering thermodynamic

cycle, thereby presenting an inventive blueprint for the agile deployment of rural low-carbon energy ecosystems. A multi-objective optimization model for rural integrated energy systems based on biogas and P2G technologies was constructed by Huo D et al. [12], who analyzed the energy flow relationships among modules but failed to fully consider the impact of seasonal fluctuations in rural energy demand on equipment capacity configuration. Zhang J et al. [13] developed an energy scheduling strategy for inter-microgrid systems with biogas power generation and a double-layer model for collaborative optimization of capacity configuration and operation of multi-microgrid systems with biogas power generation, investigating the capacity configuration of new energy systems in rural areas but without quantifying the effects of transmission losses and communication delays on inter-microgrid energy interaction. Last, Li H et al. [14] constructed a dynamic interaction model that encapsulates distributed power sources, communication networks, and control centers, offering strategic insights to bolster the resilience and security of distribution networks amidst multifaceted, heterogeneous energy landscapes.

Most researchers have not established a complete cost evaluation system. Wei F et al. [15] constructed an energy scheduling system for intelligent photovoltaic charging piles based on machine learning, optimizing scheduling through fuzzy rules to enhance photovoltaic absorption efficiency under the uncertainty of electric vehicle charging. However, the machine learning model failed to fully consider long-term effects such as battery degradation, and its adaptability to large-scale scenarios requires verification. Liu Q et al. [16] modeled the load characteristics of private electric vehicles using the Monte Carlo method, verifying the long-term economic viability of the battery swapping mode, but did not refine the dynamic changes in user charging behavior. Taking buildings as a case study, Shen B et al. [17] analyzed the impact of energy storage battery capacity and vehicle electrification rate on photovoltaic self-usage rate, determining the optimal battery configuration and investment payback period. However, the building case lacked universal analysis across building types, and the dynamic optimization mechanism of electric vehicle charging strategies and multi-scenario adaptability was insufficiently explored. Shi R et al. [18] established a double-queue dynamic optimization model for photovoltaic-storage-charging integrated charging stations but failed to consider differences in traffic flow across regions, leading to actual operating costs exceeding expectations. Huang H et al. [19] constructed a rural integrated energy system with photovoltaic-biogas collaboration but did not quantify energy losses during biogas storage, resulting in significant deviations in operational cost predictions.

A notable deficiency in the consideration of robustness is observed among some scholars in system design. Wang C [20] proposed two topologies for the direct flexible solar energy storage system in rural residential buildings, but did not explore the adaptability under complex climate and load scenarios. Carlos RP et al. [21] proposed an optimal configuration method of a biogas and photovoltaic hybrid system in rural areas, which was not included in the quantitative evaluation of power grid stability technical indicators and limited the comprehensiveness of system optimization and practical engineering adaptability. Jia Y et al. [22] proposed an "AC-DC-Storage" non-communication collaborative control strategy for voltage overlimit issues in rural low-voltage distribution networks. By establishing the mapping relationship among DC voltage, AC feeder voltage, and energy storage SOC, simulations verified that the strategy can reduce system power loss and stabilize voltage. However, it did not consider the robust control under distributed power output fluctuations in extreme weather or communication outages. Wang Y et al. [23] presented a multi-objective planning method for rural electricity-heat systems based on biomass-photovoltaic coupling, considering the virtual

energy storage of heat networks and the adjustability of agricultural loads to optimize equipment capacity configuration for enhanced economy and energy efficiency. Nevertheless, the researchers did not deeply explore the multi-energy flow coupling mechanism of electricity-heat-biomass energy, nor dynamically quantify the impact of agricultural load regulation on power grid stability.

Research has involved the integration of single energy sources in rural areas but lacks evaluation of photovoltaic-storage collaborative systems, in-depth analysis of energy storage and multi-energy complementarity, insufficient study on the integration of energy storage systems with distribution networks, inadequate exploration of complex interaction scenarios, and limited engineering verification. Accordingly, the proposed PBS-DCF building represents a novel rural building energy system that integrates PV systems, biogas power generation systems, energy storage systems, DC power supply, and flexible electricity consumption. Taking the rural renovation project as an example, a modular modeling method was used to establish an energy consumption mechanism model for the light biogas storage direct flexible building system, verifying the significant advantages of the building system in the dimensions of electricity flexibility, energy cleanliness, Operation Economy, and system stability. This building system offers a solution for the dynamic balance between energy supply and demand in rural areas, while ushering in new opportunities for rural energy transformation and sustainable development.

2. System composition and mechanistic model

2.1. System composition

The intricate architecture of the PBS-DCF building system is vividly depicted in Figure 1, with the arrows elegantly tracing the trajectory of energy flow. Embracing a DC paradigm, every device within this sophisticated system derives its power from this unified current, while the building stands proudly adorned with fast-charging piles seamlessly intertwined with a DC 750 V DC busbar [24]. The PV power generation system, the energy storage system, the biogas system, and the HVAC system are all elegantly linked to the DC busbar through the intermediary of DC/DC converters, ensuring seamless integration and efficient operation.

In a meticulous endeavor to capture the essence of each constituent component, a modular modeling approach is meticulously employed. First, models are established for each sub-module based on physical principles and mathematical relationships, respectively. Second, for the data and logical interfaces between the modules, the sub-module models are integrated to construct a complete system model. Finally, the integrated model is verified and optimized. Based on this model, we further construct the interaction model with the power grid and formulate the operation strategy, enabling the step-by-step construction of subsystem models that encompass PV power generation, biogas power generation, energy storage, HVAC, and electric vehicle charging piles.

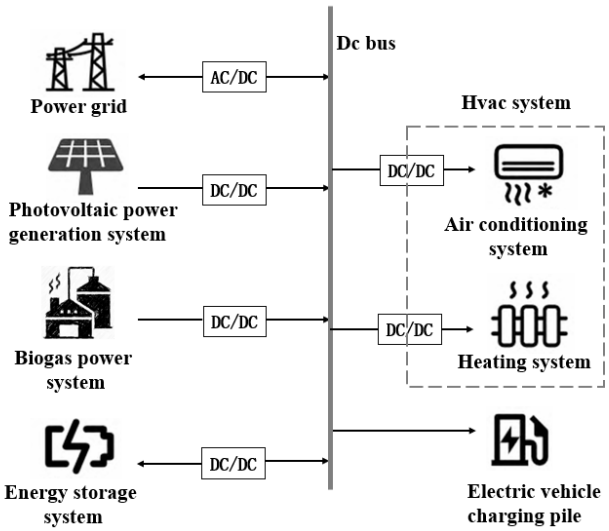

Figure 1. The system of the Photovoltaic-Biogas-Storage Direct-Current and Flexible Architecture.

2.2. Photovoltaic power generation model

Drawing inspiration from the seminal works referenced in [25,26], a PV power generation system is ingeniously designed, accompanied by a pioneering PV power generation model that aspires to mirror the actual operating conditions with unparalleled precision. The output power of this state-of-the-art PV power generation system is computed with mathematical elegance, utilizing venerable Eq (1).

$$P_{PV}^{t} = P_{STC} \cdot \frac{G_{INC}^{t}}{G_{STC}} \cdot \left[1 + \beta \cdot \left(T_{C}^{t} - T_{STC}\right)\right] \cdot \prod_{i=1}^{n} \frac{1}{1 + \gamma\left(\frac{G_{i}^{t}}{G_{STC}} - 1\right)} \tag{1}$$

$$T_{c}^{t} = T_{out}^{t} + \frac{G_{INC}^{t}}{\alpha_{T}} \cdot \left(1 - \eta_{PV}\right) - \frac{\alpha_{conv} \cdot \left(T_{c}^{t} - T_{out}^{t}\right) + \alpha_{rad} \cdot \left(T_{c}^{t} - T_{sky}^{t}\right)}{\alpha_{T}} \tag{2}$$

Among them: P_{PV}^{t} is the output power of the photovoltaic power generation system at time t (kW); P_{STC} is the rated output power under standard test conditions (kW); G_{INC}^{t} is the actual light-intensity at time (W/ m^2); G_{STC} is the reference light-intensity under standard test conditions (W/ m^2); β is the power-temperature coefficient; T_{c}^{t} is the temperature of the photovoltaic module at time t (℃); T_{STC} is the module temperature under standard test conditions (℃); γ is the non-uniformity coefficient of light-intensity; G_{i}^{t} is the light-intensity of the i-th photovoltaic module (W/ m^2); n is the number of photovoltaic modules; α_{T} is the total heat-transfer coefficient of the module; η_{PV} is the photoelectric conversion efficiency of the photovoltaic module; α_{conv} is the convective heat-transfer coefficient; α_{rad} is the radiative heat-transfer coefficient; and T_{sky}^{t} is the sky temperature at time t (℃).

2.3. Biogas power generation model

The biogas power generation system is a marvel of engineering, adept at transforming the latent chemical energy harnessed within biogas into a tangible, usable form of electrical energy. At the heart of this intricate biogas production process lies the meticulous crafting of a biogas generation model, firmly anchored in the principles of anaerobic fermentation kinetics [27]. The dance of biogas creation is orchestrated through the mathematical elegance of Eqs (3) and (4), while the reservoir of biogas storage capacity is meticulously gauged via Eq (5). Ultimately, the crescendo of this energy transformation is realized in the biogas power generation output, which is harmoniously computed through the application of Eq (6).

$$G_{bio}^{t} = k_{bio} \cdot M_{sub}^{t} \cdot f_{TS}^{t} \cdot f_{VS}^{t} \cdot \eta_{bio}^{t} \tag{3}$$

$$\eta_{bio}^{t} = \eta_{bio}^{\max} \cdot \left(-\frac{E_a}{R \cdot \left(T_{fer}^{t} - T_{ref} \right)} \right) \tag{4}$$

$$V_{bio}^{t+1} = V_{bio}^{t} + \left(G_{bio}^{t} - G_{cons}^{t} \right) \cdot \Delta t - V_{bio}^{t} \cdot \lambda_{leak} \cdot \Delta t \tag{5}$$

$$P_{gen}^{t} = Q_{bio}^{t} \cdot H_{bio} \cdot \eta_{gen} \tag{6}$$

Among them: G_{bio}^{t} is the biogas production rate at time *t* (m³/h); k_{bio} is the biogas production coefficient (m³/kg); M_{sub}^{t} is the mass of fermentation raw materials at time *t* (kg); f_{TS}^{t} is the total solid content of fermentation raw materials at time *t* (%); f_{VS}^{t} is the volatile solid content of fermentation raw materials at time *t* (%); η_{bio}^{t} is the biogas production efficiency at time *t*; $\eta_{bio}^{\max}$ is the maximum biogas production efficiency; E_a is the activation energy (kJ/(mol·℃)); R is the gas constant; T_{fer}^{t} is the fermentation temperature at time *t* (℃); T_{fer} is the reference temperature (℃); V_{bio}^{t} is the biogas storage volume; P_{gen}^{t} is the power generation capacity (kW); Q_{bio}^{t} is the biogas flow rate (m³/h); H_{bio} is the lower heating value of biogas (kJ/m³); η_{gen} is the power generation efficiency; G_{cons}^{t} is the biogas consumption rate at time *t* (m³/h); and λ_{leak} is the leakage rate of the gas storage tank.

2.4. Energy storage system model

In the grand symphony of the PBS-DCF building system, the energy storage system assumes a position of paramount importance, serving as both a virtuoso energy regulator and a steadfast backup power source. With the choice of lithium-ion batteries as the virtuous medium of energy storage [28], the model unfolds in a tapestry of battery charge-discharge characteristics, battery capacity, and the enduring narrative of battery lifespan. The ebb and flow of battery charge-discharge power are masterfully calculated through the application of Eq (7), the expanse of battery capacity is discerned via the lens of Eq (8), and the subtle erosion of battery lifespan is delicately computed using Eq (9).

$$P_B^t = \begin{cases} \eta_B^{ch} \cdot P_{ch}^t & \left(P_{ch}^t \geqslant 0\right) \\ \dfrac{P_{dis}^t}{\eta_B^{dis}} & \left(P_{dis}^t < 0\right) \end{cases} \tag{7}$$

$$C_B^{t+1} = C_B^t - \frac{P_{dis}^t \cdot \Delta t}{\eta_B^{dis} \cdot C_B^{nominal}} + \frac{P_{ch}^t \cdot \Delta t \cdot \eta_B^{ch}}{C_B^{nominal}} \tag{8}$$

$$\Delta L_B^t = \lambda_B \cdot \left(I_B^t\right)^2 \cdot \Delta t \cdot f_T^t \cdot f_{SOC}^t \tag{9}$$

Among them: P_B^t is the charging and discharging power of the battery (kW); $\eta_B^{ch}, \eta_B^{dis}$ is the charging and discharging efficiency; P_{ch}^t, P_{dis}^t are the charging and discharging powers of the battery at time *t* respectively (kW); C_B^t is the battery capacity; $C_B^{nominal}$ is the nominal capacity of the battery (kWh); Δt is the time interval; ΔL_B^t is the battery life loss; λ_B is the battery life loss factor; I_B^t is the charging and discharging current of the battery at time *t* (A); and f_T^t, f_{SOC}^t is the influence factor.

2.5. Heating, ventilation, and air conditioning system model

The HVAC load plays an important role in the operation of buildings. An air conditioning system and a heating system need to be equipped, respectively, according to different climatic conditions [29]. The output power P_{HVAC}^t of the HVAC system is calculated by Eq (10):

$$P_{HVAC}^t = \begin{cases} P_{AC}^t \cdot \alpha_{AC}^t + P_H^t \cdot \alpha_H^t & \left(\alpha_{AC}^t + \alpha_H^t \leqslant 1\right) \\ 0 & \left(\alpha_{AC}^t + \alpha_H^t > 1\right) \end{cases} \tag{10}$$

Among them: P_{AC}^t is the output power of the air-conditioning system at time t (kW); P_H^t is the output power of the heating system at time t (kW); and α_{AC}^t and α_H^t are the operation weight coefficients of the air-conditioning and heating systems at time t, with a value range of [0,1]. When the system is turned on, their values are determined according to the actual operation situation; when the system is turned off, their values are 0.

The relationship between the output power of the air-conditioning system and its cooling capacity is calculated through Eq (11), whereas the correlation between the output power of the heating system and its heat flow rate is determined via Eq (12).

$$P_{AC}^t = \frac{Q_{AC}^t}{\eta_{AC}} \tag{11}$$

$$P_H^t = \frac{1}{\eta_H} \cdot \frac{dQ_H^t}{dt} \tag{12}$$

Among them: Q_{AC}^t is the cooling capacity of the air-conditioning system at time *t* (kW); $\frac{dQ_H^t}{dt}$ is the heat flow rate delivered from the heating equipment to the room at time *t* (kW); and η_{AC}, η_H are the energy efficiency ratio and the heating efficiency, respectively.

2.5.1. Air conditioning system model

In the realm of air-conditioned environments, the intricate thermal dynamics unfolding within these spaces are elegantly encapsulated through models grounded in the fundamental principles of thermal equilibrium, as expounded upon in references [30–32]. By conceptualizing the room as a singular entity with a lumped thermal capacity, the nuanced shifts in indoor temperature T_{in}^t are intricately woven from the interplay of heat exchange between the interior and exterior realms, the cooling prowess bestowed by the air-conditioning apparatus, and the room's innate thermal resilience, all of which are meticulously calculated through the lens of Eq (13).

$$C_{room}\frac{dT_{in}^t}{dt} = \alpha_{wall}\cdot\left(T_{out}^t - T_{in}^t\right) + \alpha_{window}\cdot\left(T_{out}^t - T_{in}^t\right) + Q_{AC}^t \tag{13}$$

Among them: C_{room} is the heat capacity of the room (kJ/°C); α_{wall}, α_{window} are the heat transfer coefficients of the wall and the window, respectively (kW/°C); and T_{out}^t is the outdoor temperature at time t (°C).

2.5.2. Heating system model

The heating system, a masterful orchestrator of thermal elevation, achieves its purpose by channeling heat from the embrace of hot water or the warmth of heated air through the conduit of heat exchangers into the sanctuary of the indoor space. The output heat Q_H^t of this thermal maestro is quantified through the application of Eq (14). The ebb and flow of indoor air temperature, a dance of thermal equilibrium, are influenced by the heat generously supplied by the heating system, the ceaseless exchange of heat between the indoor and outdoor domains, and the subtle, yet significant, thermal losses of the room, all of which are harmoniously determined through the application of Eq (15).

$$Q_H^t = m_H^t \times c_H \times \Delta T_H^t \tag{14}$$

$$C_{room}\frac{dT_{in}^t}{dt} = Q_H^t - \alpha_{loss}\cdot\left(T_{in}^t - T_{out}^t\right) \tag{15}$$

Among them: Q_H^t is the output heat of the heating system; m_H^t is the flow rate of the heating medium (hot water or hot air); c_H is the specific heat capacity; ΔT_H^t is the water temperature difference; and α_{loos} is the heat loss coefficient of the room (kW/°C).

2.6. Electric vehicle charging pile model

Fast-charging electric vehicle (EV) stations can be likened to "virtual energy reservoirs" for the power grid [33]. Though they cannot directly store electrical energy, these stations exhibit functional parallels with traditional energy storage batteries. Upon connecting an EV to a charging station, the station swiftly harnesses electrical energy from the power grid and channels it into the vehicle's battery. This operation mirrors the discharge process of an energy storage battery, whereby power is supplied to external devices in a directed, high-velocity manner. The charging power of a conventional fast-charging EV station is computed via Eq (16), while the fluctuation in the EV battery's charge level, contingent upon the charging power and the duration of the charging interval, is ascertained through Eq (17).

$$P_{CP}^{t}=\begin{cases}P_{CP}^{req}\cdot\eta_{CP} & \left(Q_{EV}^{t}<Q_{EV}^{\max}\right)\\ 0 & \left(Q_{EV}^{t}\geqslant Q_{EV}^{\max}\right)\end{cases} \tag{16}$$

$$Q_{EV}^{t+1}=Q_{EV}^{t}+P_{CP}^{t}\times\Delta t\times\eta_{CP} \tag{17}$$

Among them: P_{CP}^{t} is the charging power; Q_{EV}^{t} is the current charge of the electric vehicle's battery; $Q_{EV}^{\max}$ is the battery capacity; η_{CP} is the charging efficiency; η_{CP}^{req} is the required charging power; and Δt is the charging time interval.

2.7. Power grid interaction model

In alignment with the fundamental principle of energy conservation, it is assured that within the labyrinthine power grid, irrespective of the intricate pathways, electrical energy traverses across stages like generation, transmission, distribution, and consumption, the cumulative energy magnitude remains unyieldingly constant [34]. The aggregate load power of a building system is meticulously computed through the application of Eq (18). When assessing the interaction power between the building system and the power grid at a specific time t, a pivotal distinction arises: If the collective energy supply falls short of the total load power requirement, the building system procures power from the grid, a calculation governed by Eq (19); in contrast, should the energy supply surpass the load power demand, the building system reciprocates by returning power to the grid, a process dictated by Eq (20). A state of equilibrium is achieved when the amalgamated output power of the PV generation system, the charge-discharge dynamics of the energy storage system (with negative values denoting charging and positive values signifying discharging), and the output power of the biogas generation system collectively satisfy the total load power demand. In this harmonious state, the interaction power P_{grid}^{t} between the building system and the power grid nullifies, signifying the attainment of self-sufficiency within the building system.

$$P_{load}^{t}=P_{HVAC}^{t}+P_{CP}^{t}+P_{DC}^{t} \tag{18}$$

$$P_{grid}^{t}=P_{load}^{t}-\left(P_{PV}^{t}+P_{B}^{t}+P_{gen}^{t}\right) \tag{19}$$

$$P_{grid}^{t} = \left(P_{PV}^{t} + P_{B}^{t} + P_{gen}^{t} \right) - P_{load}^{t} \tag{20}$$

Among them: P_{load}^{t} is the total load power of the building system; and P_{grid}^{t} is the interaction power between the building system and the power grid.

2.8. Operation strategy

The PV generation system takes precedence in satisfying the immediate load requirements of the building complex, which encompasses a diverse array of EV charging stations, luminous fixtures, HVAC units, and other DC electrical gadgets and apparatuses. Once these load demands are met, any surplus energy generated by the PV system is first directed towards replenishing the energy storage system, then subsequently harnessed to energize the equipment within the biogas system, and finally, if any excess persists, it is channeled back into the power grid for broader utilization.

The energy storage system steps in to discharge during instances of inadequate PV generation or when load demands peak, acting as a crucial bridge to alleviate the energy supply-demand imbalance. Its discharge strategy is meticulously orchestrated to prioritize the critical load demands of the building system before extending its support to non-critical load demands, thus ensuring the unwavering fulfillment of the building's fundamental electrical needs.

The biogas generation system operates in tandem with the biogas production rate and the dynamic energy requirements of the building system. In situations where both the PV generation system and the energy storage system are rendered insufficient to meet the load demands, the biogas generation system springs into action, generating electricity with a resolute focus on prioritizing and fulfilling the basic energy prerequisites of the building system.

3. Simulation process and solution strategy

3.1. Simulation object

Taking the residential renovation initiative in Xiaohe Village, nestled within Huaiyang District, Zhoukou City, in the heart of Henan Province, as a paradigm, the residential structure under consideration boasts a total construction area spanning approximately 235 square meters, of which around 105 square meters are designated for cooling and heating purposes. Towering at a majestic height of approximately 7.5 meters, this two-story edifice is a testament to architectural ingenuity. Blessed with abundant sunlight, the site presents an ideal canvas for the installation of PV panels, with PV modules seamlessly integrated into the roof and strategic sections of the building's exterior facade, harnessing the sun's energy with unparalleled efficiency.

3.2. Model building

Drawing upon the mathematical formulations encapsulated in model Eqs (1) through (20), an advanced, integrated simulation paradigm was meticulously engineered for a photovoltaic-biogas-energy-storage-direct-flexible architectural construct, leveraging the MATLAB computational environment. Within this framework, each constituent subsystem module is intricately linked via signal pathways, fostering seamless energy circulation and bidirectional data interchange, thus affording a

precise emulation of the building system's real-world operational dynamics. A visual schema encapsulating the architectural blueprint of the holistic system simulation model is elegantly presented in Figure 2.

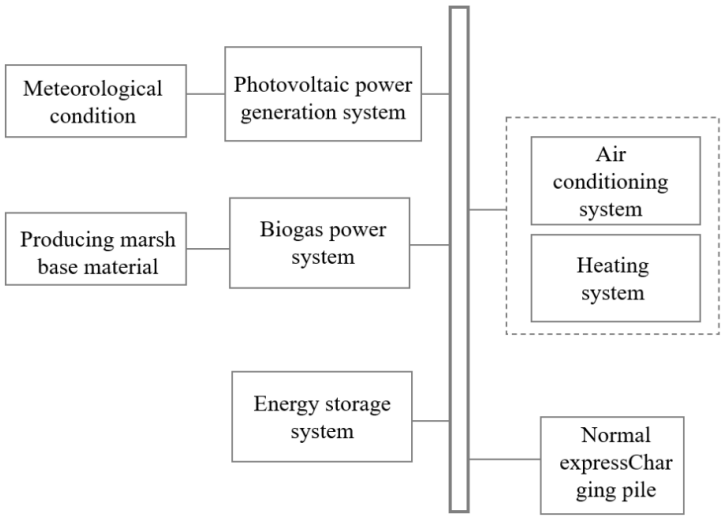

Figure 2. Overall simulation diagram of the Photovoltaic-Biogas-Energy storage direct-current flexible building.

3.3. Parameter setting

3.3.1. Basic data

Conforming to the quotidian rhythms and energy consumption patterns intrinsic to the inhabitants of Xiaohe Village, the zenith periods of electrical demand are delineated as spanning from 8:00 AM to 12:00 PM and from 3:00 PM to 11:00 PM, epochs during which the exigencies for electrical energy utilization manifest. The parameters of the photovoltaic system are shown in Table 1.

Table 1. Photovoltaic system parameters.

Parameters	Take the value
Rated installed capacity/kW	30
Rated output power of the unit/kW	2.5
Power temperature coefficientβ/℃	−0.35%
First-year decline rate	2.5%
Service life/a	20
Power generation efficiency	85%

Guided by the meteorological nuances and topographical specifics of the locale, as well as the regulatory benchmarks delineated in GB 50736—2012, "Code for Design of Heating, Ventilation, and Air Conditioning of Civil Buildings" [35], the thermostatic parameters governing indoor environmental conditions across the annual climatic spectrum are judiciously established, ensuring the

attainment of optimal thermal comfort for the building's occupants, as comprehensively catalogued in Table 2.

Table 2. Indoor temperature settings for the four seasons (°C).

Season	Spring	Summer	Autumn	Winter
Range of Temperature	[15,20]	[20,25]	[15,20]	[18,22]

Drawing upon architectural design and construction documentation, detailed information regarding the areas, materials, and thermal conductivity coefficients of the building's exterior walls, windows, roofs, and ancillary components was meticulously extracted. This data was subsequently harnessed to compute the building's equivalent thermal resistance, providing a comprehensive understanding of its thermal performance.

The energy storage system's capacity is strategically bifurcated into rigid and flexible segments. The rigid part refers to the fixed capacity set in the energy storage system to meet the deterministic and essential basic load or reliability requirements that must be guaranteed. The flexible part refers to the capacity in the energy storage system that can dynamically adjust charging and discharging according to real-time supply and demand changes, electricity price signals, or system dispatching instructions. The rigid capacity is meticulously calculated in alignment with GB/T33589—2017 "Technical Regulations for Microgrid Connection to Power Systems" [36] while taking into account the unique attributes of this particular building. Consequently, the rigid load segment was quantified at 60 kW·h, whereas the flexible capacity is designated at 200 kW·h, culminating in an aggregate energy storage system capacity of 260 kW·h. The parameters of the energy storage equipment are shown in Table 3.

Table 3. Parameters of energy storage equipment.

Parameters		Take the value
Rigid state of charge	Maximum value	95%
	Minimum value	50%
Flexible state of charge	Maximum value	90%
	Minimum value	20%
Rated power/kW		52
Rated capacity/kW·h		260
Charging and discharging energy efficiency		90%
Operating temperature/°C		−20–45

Within the architectural premises, a 30 kW DC fast-charging pile was installed, with its operational usage time proportionately set at 30%, thereby catering to the electric vehicle charging requirements of the occupants. The relevant parameters of electric vehicles are shown in Table 4.

Table 4. Parameters related to electric vehicles.

Parameters	Indicator
Rated capacity of the battery/kWh	80
The maximum terminal voltage of the battery/V	380
Rated voltage of the battery/V	320
Maximum charging current/A	80
Termination current/A	8
Energy consumption of air conditioning/kW	4
Operating energy consumption [/kWh·(km)$^{-1}$]	1.5

3.3.2. Meteorological conditions

By delving into the extensive database of the National Meteorological Information Center, a wealth of historical data pertaining to outdoor temperature and solar irradiance spanning the past five years in this region was procured. Through rigorous analysis, insightful data on outdoor temperature fluctuations and photovoltaic power generation for a quintessential summer day were distilled, as graphically depicted in Figure 3. The selection criteria for typical summer days were based on the time range of working days with an average temperature of $\geq$22 ℃ in the summer pentad, a daily average temperature of 28–36 ℃, a daily temperature difference of $\geq$8 ℃, and a sunshine duration of $\geq$7 hours, with few cloudy and sunny days.

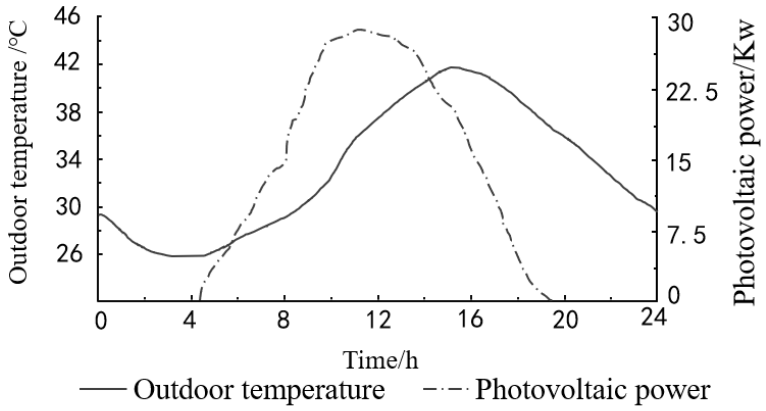

Figure 3. Variations of outdoor temperature and photovoltaic power generation on a typical summer day.

3.3.3. Evaluation indicators

To comprehensively evaluate the performance of the photovoltaic-biogas-energy storage-DC-flexible building system, daily electricity costs C_{grid} were used as the basis for economic evaluation indicators to calculate the economic benefits during the operation of the building system, as computed by Eq (21). The cleanliness evaluation index of this building system included the electricity extraction ratio (μ) as the main basis, and a lower electricity extraction ratio signified a reduced reliance of the

building system on the power grid, as calculated by Eq (22).

$$C_{grid} = \sum_{t=1}^{24} C_{TOU}^{t} \cdot P_{grid,i}^{t} \cdot \Delta t - \sum_{t=1}^{24} C_{FI}^{t} \cdot P_{grid,o}^{t} \cdot \Delta t \tag{21}$$

$$\mu = \frac{\sum_{t=1}^{24} P_{grid,i}^{t}}{\sum_{t=1}^{24} P_{load}^{t}} \tag{22}$$

Among them: C_{TOU}^{t}, C_{FI}^{t} respectively represent the electricity selling price and feed-in tariff of the power grid at time t (yuan/kWh); $P_{grid,i}^{t}, P_{grid,o}^{t}$ respectively represent the power drawn from the power grid and the power fed into the power grid by the building system at time t (kW); and represents the time step, which is set as 5 minutes (i.e., 1/12 h).

The segmented electricity tariff and feed-in tariff are illustrated in Figure 4. Throughout the day, electricity prices were at their peak during the periods of 11:00 AM–2:00 AM and 6:00 PM–10:00 PM, during which the stored electricity from the energy storage system should be utilized to the fullest extent possible. The feed-in tariff adheered to the local guiding electricity price.

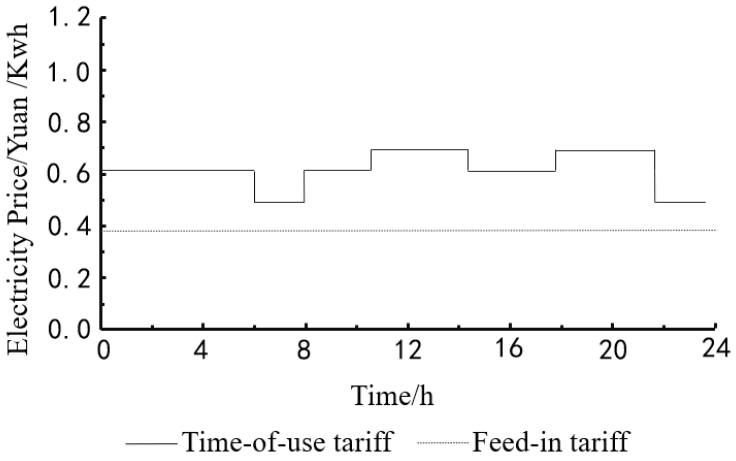

Figure 4. Diagram of time-of-use electricity prices and feed-in tariffs throughout the day.

The fluctuation range of indoor temperature and the peak power intake were taken as the main basis for the stability index of the building system.

4. Simulation results and analysis

4.1. Electricity consumption flexibility

A comparative analysis was conducted between the operational performance of the PBS-DC-FAS and that of a conventional building system on a quintessential summer day, aiming to substantiate the superior electricity usage flexibility inherent in the PBS-DC-FAS. The specific configuration of the building is shown in Table 5.

Table 5. Comparison of building configurations.

	Traditional building systems	PBS-DC-FAS
Photovoltaic system	No installation	Installation
Biogas system	No installation	Installation
Energy storage system	No installation	Installation
Heating, ventilation, and air conditioning system	Fixed-Frequency operation	Variable-Frequency Operation

The traditional building system, characterized by its unwavering power consumption, struggles to maintain indoor temperatures within a desirable range due to its susceptibility to outdoor environmental fluctuations. During periods of heightened electricity demand, the inadequacy of photovoltaic power generation necessitates the procurement of electricity at elevated prices, whereas any surplus energy is divested to the grid at a discounted rate. Specifically, between 10:00 AM and 4:00 PM, when outdoor temperatures soar, the air-conditioning unit of the traditional building system, operating at a preset frequency, is unable to dynamically adapt its power output in response to actual cooling requirements, leading to uncomfortably high indoor temperatures that not only compromise occupant comfort but also exacerbate the strain on the power grid.

Conversely, the PBS-DC-FAS harnesses variable-frequency technology, facilitating real-time modifications to its power output in accordance with indoor and outdoor temperature variations, as well as the availability of solar energy. During daylight hours characterized by intense sunlight and elevated temperatures, the air-conditioning system operates at an elevated frequency to augment cooling capacity, with photovoltaic power generation taking precedence to satisfy load demands, and any surplus energy being stored within the energy storage and biogas systems. During the off-peak electricity hours of the night, the energy storage system is replenished, and the biogas system generates gas as required for storage or power generation. Between 12:00 PM and 2:00 PM, when outdoor temperatures peak at 35 °C, the air-conditioning system of PBS-DC-FAS automatically escalates its operating frequency to amplify cooling output, while simultaneously leveraging the synchronized power supply from the energy storage and photovoltaic power generation systems to uphold indoor temperatures at approximately 25 °C, thereby significantly augmenting occupant thermal comfort. Moreover, this system optimizes electricity consumption strategies by capitalizing on off-peak electricity during nocturnal hours, thereby enhancing electricity usage flexibility and fostering a "reciprocal interaction between supply and demand".

4.2. Operational economy

Taking daily electricity expenses as the yardstick for economic evaluation, the variations in daily electricity costs compared to traditional buildings are vividly depicted in Figure 5. Under the prevailing energy management strategy, the traditional building system has relatively steep daily electricity expenses. The PBS-DC-FAS achieves cost reduction through optimized energy scheduling. During a quintessential summer day, the energy storage system charges during the off-peak electricity tariff periods at night, while the biogas system harnesses self-produced biogas for electricity generation, thus curbing grid electricity consumption. Calculations reveal that the PBS-DC-FAS substantially curtails daily electricity expenses and exhibits commendable economic performance.

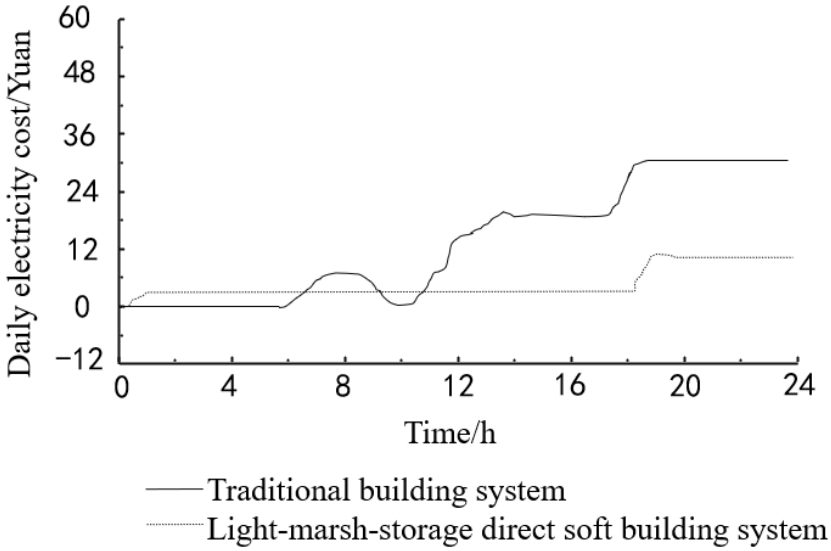

Figure 5. Changes in the daily electricity costs of the building.

A deeper dive into the contributions of disparate energy sources to operational economy was undertaken. Within the PBS-DC-FAS, PV power generation provides a copious supply of electricity during daylight hours with ample sunlight, diminishing reliance on the grid. The energy storage system capitalizes on electricity tariff arbitrage by charging during off-peak tariff periods and discharging during peak tariff periods. The biogas system taps into the wealth of rural biomass resources to produce biogas for electricity generation, not only slashing waste disposal costs but also yielding supplementary electricity. During the summer, PV power generation meets the lion's share of daytime electricity demand, the energy storage system stores electricity during off-peak tariff periods at night and releases it during daytime peak electricity consumption periods, effectively mitigating grid electricity costs. Concurrently, the electricity generated by the biogas system further diminishes dependence on external energy sources and augments the system's economic efficiency.

4.3. Energy cleanliness

The electricity extraction ratio and the proportion of clean energy were harnessed to gauge energy cleanliness, as presented in Table 6. The traditional building system grapples with a high electricity procurement ratio and a paltry proportion of clean energy catering to the load. The PBS-DC-FAS makes the most of PV power generation and biogas power generation; the electricity extraction ratio has decreased by 24.8% compared to the traditional system, meeting the daily operation's power self-sufficiency. Moreover, augmenting the proportion of clean energy, curtailing daily electricity purchases from the grid, effectively bolstering energy self-sufficiency, and curbing carbon emissions are observed.

Table 6. Cleanliness indicators of building energy use.

	Traditional building systems	PBS-DC-FAS
Electricity Extraction Ratio	63.2%	15.7%
Photovoltaic Power Generation/kW·h		54
Biogas Power Generation/kW·h		15
Battery Charging Capacity/kW·h		10
Battery Discharging Capacity/kW·h		5
Total Electricity Consumption/kW·h	80.5	75.8

On a quintessential summer day, the output power of the PV power generation system dances in harmony with the sun's radiant intensity. During the sun-drenched hours from 9:00 to 17:00, the PV system adeptly fulfills the majority, if not all, of the building's energy demands, with any excess electrical energy being judiciously stored or harnessed to power the equipment integral to the biogas system. The biogas system, a master of its craft, orchestrates the steady production of biogas for power generation, harmoniously complementing the PV system's output. As twilight descends and sunlight wanes, the biogas power generation system springs into action as needed, seamlessly supplementing the power supply to ensure the unwavering stability of the building system, thereby elevating the efficiency and dependability of clean energy utilization.

4.4. System stability

System stability stands as the linchpin of operational reliability and user satisfaction. The PBS-DC-FAS forges stability through the artful orchestration of multi-energy dispatching. In stark contrast to traditional building systems, which are prone to erratic fluctuations in peak power draw and place undue strain on the power grid, the PBS-DC-FAS employs both the energy storage and biogas systems as steadfast buffers, effectively taming power fluctuations and significantly curbing peak power draw. The peak power extraction has decreased by 36.6% compared to traditional building systems, as shown in Table 7. Moreover, this system fosters an environment of enhanced indoor temperature stability, catering more adeptly to human thermal comfort needs.

Table 7. Peak power extraction parameter of building.

	Traditional building systems	PBS-DC-FAS
Peak Power Extraction /kW	25.4	16.1

When confronted with the whims of sudden weather shifts or load fluctuations, the PBS-DC-FAS stands poised and ready, responding with agility and precision. The energy storage system springs into action at a moment's notice, discharging to bridge any power gaps, while the biogas system adeptly modulates its power generation output in accordance with pre-established strategies, ensuring the uninterrupted and stable operation of critical building loads. This proactive approach not only shields equipment from potential damage or functional anomalies stemming from energy supply fluctuations but also bolsters the system's resilience in the face of uncertainty, fortifying its stability and reliability.

5. Conclusions

In this study, we focus on the rural Photovoltaic-Biogas-Storage Direct-Current and Flexible Architecture System. Through modular modeling, an overall simulation model including photovoltaic power generation, biogas power generation, energy storage, heating, ventilation, and air conditioning, and charging stations is constructed. The simulation verification is carried out in conjunction with the renovation project of Xiaohe Village in Zhoukou, Henan Province. The technical advantages of the system were verified from the dimensions of electricity flexibility, economy, cleanliness, and stability. The major findings and contributions are summarized as follows:

1) A modular integrated model is constructed to achieve the organic integration of photovoltaic power generation, biogas power generation, stratified energy storage (60 kWh rigid capacity/200 kWh flexible capacity), and variable-frequency heating, ventilation, and air conditioning systems. The case simulation in Xiaohe Village, Henan, shows that the proposed light-biogas-storage direct flexible system can achieve a photovoltaic self-consumption rate of 84.3%, which is 47.5% higher than that of the traditional system, effectively solving the problem of supply-demand mismatch in rural power grids.

2) Multi-dimensional optimization results of system performance show that through the coordination of electrical energy storage with photovoltaics and biogas power generation, the daily electricity cost is reduced by 66.7%, the grid dependency ratio decreases from 53.2% to 18.7%, the clean energy supply accounts for 85.3%, and carbon emissions are reduced by 78.3%. Moreover, the peak power consumption decreases by 36.6% (from 25.4 kW to 16.1 kW), balancing economy, cleanliness, and operational stability.

3) The innovative multi-energy complementary architecture uses biogas as a seasonal complementary energy source for photovoltaics, overcoming the intermittent nature of a single energy source. Based on the load characteristics of rural areas, a hierarchical energy storage system is designed. The rigid capacity is utilized to ensure basic power supply, while the flexible capacity is used to smooth out load fluctuations. The full life cycle model incorporates photovoltaic degradation (first-year loss of 2.5%) and biogas storage loss (leakage rate of 3%), providing a quantitative basis for investment in rural energy projects.

4) Future research will entail intelligent control of biogas fermentation temperature under extreme weather and collaborative optimization of the light-biogas-storage system with rural microgrids. This system provides a technical paradigm for the large-scale promotion of zero-carbon villages, holding significant practical implications for advancing global rural energy transition and achieving the "double carbon" goals.

Use of AI tools declaration

We confirm that no artificial intelligence assistance was utilised at any stage of this work—encompassing research design, data collection and analysis, interpretation of findings, or manuscript composition. All processes were conducted wholly independently by the authors.

Acknowledgements

This work was supported by the International Science and Technology Cooperation Project in Henan Province (Key Project) [Grant number 241111521200]; the Science and Technology Research Project in Henan Province [Grant number 242102321099]; The Open fund of Henan Province Engineering Research Center of Efficient use of new energy of low carbon technologies [Grant number JDDT2024-21]; the Plan for Enhancing the Strength of Advantageous Disciplines in Zhongyuan University of Technology: "Civil Engineering" [Grant number SD202423].

Conflict of interest

The authors declare that the research was conducted in the absence of any commercial, financial, or personal relationships that could be construed as a potential conflict of interest.

Contributions

Author Yingjie Wang: conceptualization, methodology, formal analysis, writing—review & editing. Author Shijie Li: writing—original draft, formal analysis, visualization. Author Yi Zhao: conceptualization, funding acquisition, supervision, project administration. Author Shuailei Kang: investigation, formal analysis, writing—review & editing. Author Guanghui Chu: investigation, visualization, writing—review & editing.

References

1. Zhi Y, Sun T, Gao D, et al. (2024) Achieving net zero energy heating by integrating the building envelope as a thermal battery. *iScience* 27: 109892. https://doi.org/10.1016/j.isci.2024.109892
2. Tang W, Wang Z, Zhang L (2024) Morphological characteristics and key technologies of new rural energy system under the background of green and low-carbon energy transition. *Distrib Util* 41: 88–99.
3. Zhao A, Jiao Y, Yu J, et al. (2024) Design optimization of zero-carbon integrated energy system for time-zone energy demand of rural buildings. *Acta Energ Sol Sin* 45: 369–378. https://doi.org/10.19912/j.0254-0096.tynxb.2023-0378
4. Liu R, Zheng ZJ, Sun Y, et al. (2024) Collaborative planning of multivariate energy systems adapted to typical rural scenarios. *Proc CSU-EPSA* 36: 150–158. https://doi.org/10.19635/j.cnki.csu-epsa.001378
5. Li SG, Zhu CX, Zhang LH, et al. (2025) Multi-Agent collaborative operation optimization model for rural clean energy multi-energy complementary system. *Syst Eng Theory Pract*: 1–19. Available from: https://link.cnki.net/urlid/11.2267.N.20250306.1408.002.
6. Jiang Y (2021) Photovoltaic-Energy Storage-Direct-Current-Flexible: A new building power distribution system to assist in achieving zero-carbon electricity. *HVAC* 51: 1–12. https://doi.org/10.19991/j.hvac1971.2021.10.001
7. Allen J, Halberstadt A, Powers J, et al. (2020) An optimization-based supervisory control and Coordination Approach for solar-load balancing in building energy management. *Maths* 8: 1215. https://doi.org/10.3390/math8081215

8. Cao XM, Chen XL, Huang H, et al. (2024) Multi-Time scale optimal scheduling of a photovoltaic energy storage building system based on model predictive control. *Energy Eng* 121: 1067–1089. http://dx.doi.org/10.32604/EE.2023.046783
9. Massano M, Macii E, Lanzini A, et al. (2023) A GIS open-data co-simulation platform for photovoltaic integration in residential urban areas. *Engineering* 26: 198–213. https://doi.org/10.1016/j.eng.2022.06.020
10. Dong JD, Huang LZ, Jiang JJ, et al. (2024) Dynamic optimal power flow calculation of three-phase four-wire low-voltage distribution network with photovoltaic and energy storage. *Southern Power Syst Tech* 18: 1–13. Available from: https://link.cnki.net/urlid/44.1643.tk.20241216.1128.005.
11. Tang AH, Wang QM, Zhou M, et al. (2024) Research on the low-carbon dispatch model of the rural "Chemistry-Thermal-Electricity" coupling system considering biogas power generation and the new thermal cycle. *Proc CSEE* 61: 1–14. https://doi.org/10.13334/j.0258-8013.pcsee.240273
12. Huo DY, Zhang LM, Liu N, et al. (2025) Multi-objective optimal configuration of rural integrated energy system based on biogas and P2G. *J Agric Univ Hebei* 48: 108–117. https://doi.org/10.13320/j.cnki.jauh.2025.0030
13. Zhang JL, Cheng J (2025) Double-Layer optimization model for capacity configuration of rural multi-microgrid system with biogas power generation. *Electr Power Constr*, 1–16. Available from: https://link.cnki.net/urlid/11.2583.tm.20250516.1036.010.
14. Li H, Zhu H, Yang ZH, et al. (2019) Research on the integrated modeling method of the cyber-physical system in the distribution network and its interaction mechanism. *Electr Power* 52: 17–24. https://doi.org/10.11930/j.issn.1004-9649.201808134
15. Wei F, Xu D, Chen X, et al. (2025) Research on energy scheduling system of intelligent photovoltaic charging pile based on machine learning. *Renewable Energy Res* 43: 268–274. https://doi.org/10.13941/j.cnki.21-1469/tk.2025.02.011
16. Liu Q, Wang CM, Xie N, et al. (2024) Planning method of charging and battery swapping stations considering differentiated behavioral characteristics of electric vehicles in new distribution systems. *Smart Power* 52: 18–24.
17. Shen BQ, Wang ZL, Chen Q, et al. (2024) Research on strategies for improving building photovoltaic absorption rate: Application analysis based on energy storage batteries and electric vehicles. *Build Sci* 40: 134–141. https://doi.org/10.13614/j.cnki.11-1962/tu.2024.04.15
18. Shi RF, Chang T, He Z, et al. (2025) Research on planning method of photovoltaic-storage-charging integrated electric vehicle charging station. *Acta Energ Solaris Sin* 46: 109–118. https://doi.org/10.19912/j.0254-0096.tynxb.2024-0023
19. Huang HX, Liang R, Li JX, et al. (2024) Operation optimization of rural integrated energy system under photovoltaic-biogas collaboration. *Proc CSEE*: 1–15. https://link.cnki.net/urlid/11.2107.tm.20240914.1032.006
20. Wang CL, Xiao T, Li SJ, et al. (2024) Performance investigation of PEDF system applied in rural areas. *Electr Power* 57: 160–169. https://doi.org/10.11930/j.issn.1004-9649.202303094
21. Roldán-Porta C, Roldán-Blay C, Dasí-Crespo D, et al. (2023) Optimising a biogas and photovoltaic hybrid system for sustainable power supply in rural areas. *Appl Sci* 13: 2155–2165. https://doi.org/10.3390/app13042155

22. Jia YJ, Li T, Xi DM, et al. (2025) Voltage overlimit control strategy for rural low-voltage distribution networks with "AC-DC-Storage" non-communication collaboration. *Autom Electr Power Syst*: 1–16. http://dx.doi.org/10.7500/AEPS20241106005
23. Wang YL, Han X, Liu C, et al. (2023) Planning of rural electricity-heat integrated energy system based on biomass-photovoltaic coupling utilization. *Electr Power Constr* 44: 1–14. https://doi.org/10.12204/j.issn.1000-7229.2023.03.001
24. Yu MF, Zhou JX, Han SW, et al. (2024) Modeling and simulation research on the overall characteristics of the photovoltaic-energy storage-direct-current-flexible building. *Build Sci* 40: 142–149. https://doi.org/10.13614/j.cnki.11-1962/tu.2024.04.16
25. Molnár G, Cabeza LF, Chatterjee S, et al. (2024) Modelling the building-related photovoltaic power production potential in the light of the EU's solar rooftop initiative. *Appl Energy* 360: 122708. https://doi.org/10.1016/j.apenergy.2024.122708
26. Wang G, Feng GH, Li XL, et al. (2023) Design optimization integrating energy, economic, and environmental evaluation of a hybrid solar heating system for detached buildings in rural China. *J Build Eng* 73: 106692. https://doi.org/10.1016/j.jobe.2023.106692
27. Meisam M, Augustine A, Francisco J, et al. (2023) Wind, solar and biogas power generation in water-stressed areas of Morocco considering water and biomass availability constraints and carbon emission limits. *Energy* 282: 128756. https://doi.org/10.1016/j.energy.2023.128756
28. Tao YJ, Yang X, Zhang MX, et al. (2024) Research on the improved droop control strategy of hybrid energy storage in a DC microgrid based on MPC. *Smart Power* 52: 89–97. https://doi.org/10.20204/j.sp.2024.11012
29. Pei FX, Liu Y, Wu T, et al. (2024) A two-layer optimization control strategy for HVAC systems with coordinated consideration of air quality and thermal comfort. *Autom Electr Power Syst* 48: 151–160. https://doi.org/10.7500/AEPS20231205006
30. Mao CN, Ye MS, Li ZW, et al. (2024) An algorithm for self-generation of optimization strategies for central air conditioning systems based on a multi-level data-driven model. *Build Sci* 40: 164–172. https://doi.org/10.13614/j.cnki.11-1962/tu.2024.12.18
31. Wang M, Wang Z, Geng Y, et al. (2022) Interpreting the neural network model for HVAC system energy data mining. *Build Environ* 209: 108449. https://doi.org/10.1016/j.buildenv.2021.108449
32. Zhao J, Yang ZL, Shi LY, et al. (2024) Photovoltaic capacity dynamic tracking model predictive control strategy of air-conditioning systems with consideration of flexible loads. *Appl Energy* 356: 122430. https://doi.org/10.1016/j.apenergy.2023.122430
33. Mei ZY, Que ZC, Qiu H, et al. (2023) Optimizing the configuration of electric vehicle charging piles in public parking lots based on a multi-agent model. *Phys A* 632: 129329. https://doi.org/10.1016/j.physa.2023.129329
34. Djidimbélé R, Ngoussandou BP, Kidmo DK, et al. (2022) Optimal sizing of hybrid Systems for power loss reduction and voltage improvement using PSO algorithm: Case study of Guissia rural grid. *Energy Rep* 8: 86–95. https://doi.org/10.1016/j.egyr.2022.06.093
35. Ministry of Housing and Urban-Rural Development of the People's Republic of China (2012) GB50736—2012 Design Code for Heating, Ventilation and Air Conditioning of Civil Buildings. Beijing: China Architecture & Building Press, 7–8. Available from: https://ebook.chinabuilding.com.cn/zbooklib/bookpdf/probation?SiteID=1&bookID=60351.

36. General Administration of Quality Supervision, Inspection and Quarantine of the People's Republic of China, Standardization Administration of the People's Republic of China (2017) GB/T 33589—201 Technical Specifications for the Connection of Microgrids to the Power System. Beijing: Standards Press of China, 2. Available from: http://c.gb688.cn/bzgk/gb/showGb?type=online&hcno=9B91CA52B266AB7BD423577F9320793E.

AIMS Press